

## Ray-tracing model and Monte Carlo simulation for the design of the concentrating solar simulator reflector

Marco Bortolini,<sup>1</sup> Mauro Gamberi,<sup>2</sup> Alessandro Graziani<sup>3</sup>  
<sup>1,2,3</sup>Department of Management and Engineering, University of Padova, Italy

**Abstract:** Solar simulators are common laboratory devices to artificially reproduce the Sun emission spectrum. Their use in optic tests allows to study the effect of the solar radiation on both materials and components. This paper focuses on the effective design of the ellipsoidal reflector for concentrating solar simulators. A ray-tracing analytic model integrated to Monte Carlo simulation is proposed as an effective approach to optimize the reflector geometric configuration and to maximize the target incident radiation level and flux distribution. The developed model reproduces the ray trajectories from the source to the target and it includes the physical and optic phenomena affecting the light rays, e.g. absorption, deviation, reflection, distortion, etc. A realistic case study for the effective design of the ellipsoidal reflector for a single source small scale simulator, integrating a commercial xenon short arc lamp, is proposed to both validate and apply the proposed approach. Several scenarios are tested and the main obtained evidences are summarized.

**Keywords:** Ellipsoid, Monte Carlo simulation, Ray-tracing, Reflector surface, Solar simulator.

### I. INTRODUCTION

Solar simulators provide a luminous flux approximating natural sunlight spectrum. Their basic structure includes a metal support frame, a light source, e.g. high flux arc lamp with power supplier, igniter and electronic load, and a reflective surface to properly orient the emitted rays lighting the target area. The reflector shape allows the system to generate a concentrated or non-concentrated light beam through an ellipsoidal or parabolic reflector. Fig. 1 shows a 3D scheme of a concentrating solar simulator, highlighting its functional modules.

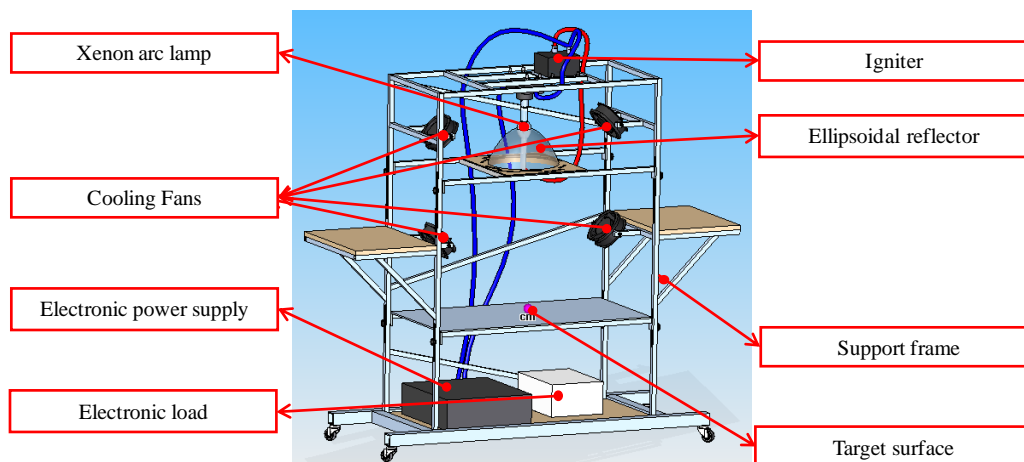


Figure 1: Single Source Solar Simulator, Functional Modules.

The relevance of such systems, in laboratory tests and analyses, is frequently discussed by the recent literature presenting several applications for a wide set of research fields. Petrash et al. [1] both review the topic and describe a 11000 suns high-flux solar simulator. Domínguez et al. [2, 3], Pravettoni et al. [4], Rehn and Hartwig [5], Hussain et al. [6] and Meng et al. [7] present different studies about the design and development of high flux solar simulators applied to both concentrating and non-concentrating photovoltaic systems.

Amoh [8] and Meng et al. [9] describe the design of solar simulators to test multi-junction solar cells for terrestrial and space applications. Kreuger et al. [10] develop a 45kW solar simulator for high-temperature solar thermal and thermo-chemical researches, while Codd et al. [11] present a low cost high flux simulator to study the optical melting and light absorption behavior of molten salts. All contributions focus on the relevance of the proper design of the system to achieve high performances in both flux intensity and uniformity on the target area. The mirror reflective surface represents a crucial component to gain these purposes. An accurate shape design and simulation of the physical and optic properties is essential before the simulator construction [12].

Ray-tracing algorithms are recognized as effective approaches to test the performances of different configurations of the reflective surface [1, 13-15].

This paper presents a ray-tracing model integrated to a Monte Carlo simulation to effectively design the ellipsoidal reflector of a single source concentrating solar simulator. The proposed model analytically reproduces the ray trajectories

from the source to the target and it includes the physical and optic phenomena and the distortions affecting the light rays. Furthermore, the ray-tracing model integration to the Monte Carlo simulation allows to test and compare several configurations of the reflector geometry and to study the most performing shape. This paper discusses such an approach and applies it to a realistic case study. The design of the reflector for a small scale solar simulator based on a commercial xenon short arc lamp is assessed. Particularly, the description of the implemented steps is provided together with the analysis of the simulated scenarios. Finally, the major outcomes are presented and properly commented.

The proposed approach goal is to support the designer of solar simulator optic systems with an integrated and easy-use method to rapidly test a system geometry before the prototyping phase and laboratory validation. An integrated approach to gain this purpose is of strong interest for both scientists and practitioners and its development is frequently encouraged.

The reminder of the present paper is organized as follows: Section II describes the steps of the developed ray-tracing model, while Section III introduces the Monte Carlo analysis and the aforementioned case study to design the ellipsoidal reflector of a single source concentrating solar simulator. The obtained results are presented and widely discussed in Section IV. Finally, Section V concludes this paper providing suggestions for further research.

## II. RAY-TRACING MODEL

In geometrical optics, the foci of an ellipsoid of revolution are conjugate points [1]. If no distortion effects occur, each ray emitted by a punctiform source located in one of the foci passes through the other after a single specular reflection. According to this principle, the concentrating solar simulators are designed. The light source, i.e. the yellow spot in Fig. 2, reproducing the Sun emission spectrum and the target surface, i.e. the blue spot in Fig. 2, are located in correspondence of the two foci of an ellipsoidal surface, while the reflector lies on a portion of such an area and it is limited by a truncation section as depicted in Fig. 2 presenting the overall geometry of the system.

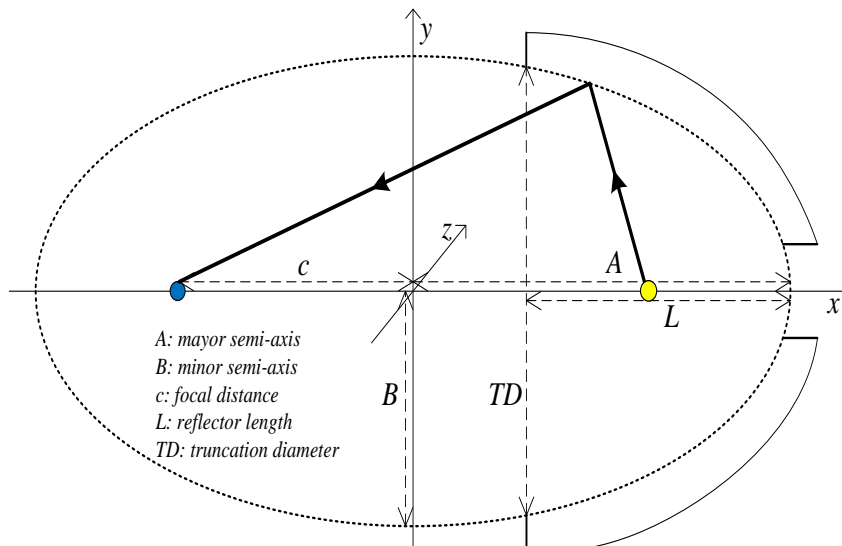


Figure 2: Single Source Solar Simulator Geometry and Notations.

Considering the operative contexts, the following conditions and phenomena contribute to reduce the global system radiation transfer efficiency, expressed as the ratio between the light flux that reaches the target and the global emitted flux.

- The finite area of the light source;
- The absorption phenomena caused by the presence of the quartz bulb, the electrodes and the reflective surface;
- The deviation and distortion phenomena caused by the specular dispersion errors of the reflective surface;
- The losses caused by the rays falling out of the reflector shape.

Such conditions cannot be neglected in the solar simulator design. Their impact in reducing the system performances is strongly correlated to the features of the emitting source, the target shape and, particularly, to the reflector characteristics. From this perspective, a model approaching this issue from an analytic point of view is of crucial interest.

The proposed ray-tracing approach faces this topic and it studies the ray trajectories, predicting the system global performances for a given configuration of the source, the reflector and the target surface. The next Fig. 3 shows the ray-tracing model flow-chart. It summarizes the step sequence of the proposed approach together with the stages in which the losses in the transfer efficiency generally occur.

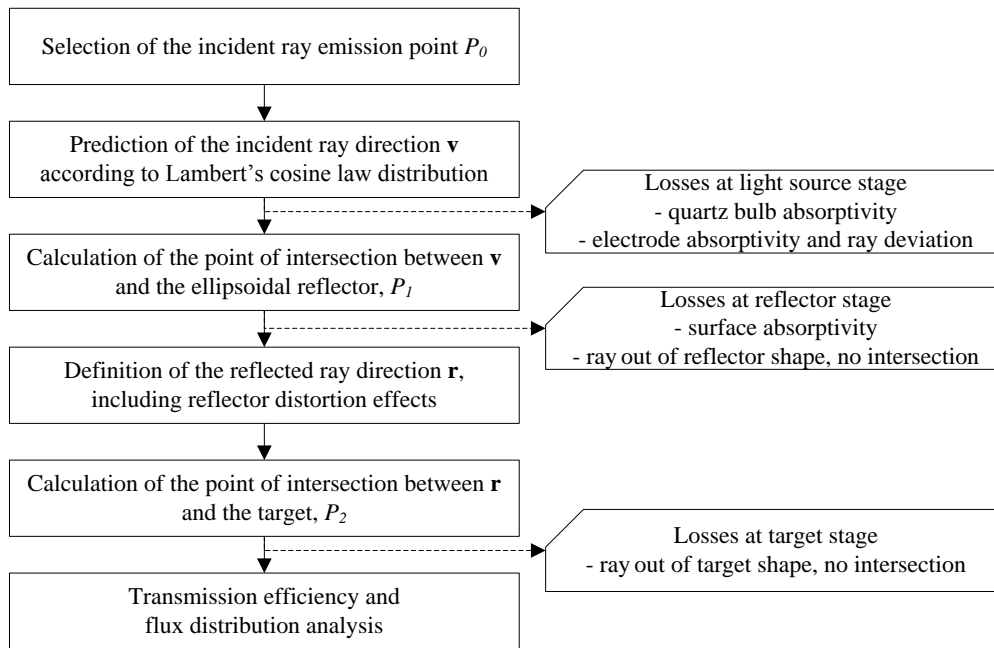


Figure 3: Ray-Tracing Model Flow-Chart.

According to the major literature [1, 2, 10] the light source is assumed to emit isotropic radiation uniformly from its surface. Consequently, the emission point,  $P_0$ , is randomly located on the whole source surface. The incident ray direction,  $\mathbf{v}$ , is defined following the Lambert's cosine law distribution, as in (1) [16].

$$\mathbf{v} \times \mathbf{n} = \cos(\sin^{-1}\sqrt{U}) = \sqrt{1-U} \quad (1)$$

where  $\mathbf{n}$  is the normal direction to the emitting surface, in  $P_0$ , and  $U$  a random number drawn from a  $[0, 1]$  uniform distribution. The quartz bulb and electrodes absorption phenomena are considered introducing two coefficients, i.e. the bulb and the electrodes absorption coefficients, reducing the emitted rays and decreasing the system efficiency, i.e. the losses at the light source stage.

For each emitted ray, the point of intersection with the ellipsoidal surface,  $P_1$ , is calculated. If  $P_1$  falls out of the reflector shape or it falls in the hole, close to the ellipsoid vertex, necessary to install the light source, the ray is considered lost and the process finishes. Otherwise, two possibilities occur. Generally, the mirror reflects the ray but, in few cases, an absorption phenomenon occurs and the ray is not reflected at all. In such a circumstance, modeled considering a further absorption coefficient, the process ends, i.e. the losses at the reflector stage.

Finally, considering the reflected rays, their direction,  $\mathbf{r}$ , is calculated. The vector  $\mathbf{r}$  is affected by the distortion effects caused by the specular dispersion errors of the reflective surface. As widely discussed by Cooper and Steinfeld [15], the geometric surface errors modify the normal vector,  $\mathbf{k}$ , to the ellipsoid surface. The authors identify two angular components of the dispersion error, i.e. the azimuthal angular component,  $\theta_{err}$ , and the circumferential component,  $\varphi_{err}$ . By applying the, so called, Rayleigh method they outline the following expressions to estimate them:

$$\theta_{err} = \sqrt{2} \cdot \sigma_{err} \cdot \sqrt{-\ln U} \quad (2)$$

$$\varphi_{err} = 2\pi U \quad (3)$$

where  $\sigma_{err}$  is the standard deviation of the dispersion azimuthal angular error distribution, including all distortion effects, and  $U$  a random number drawn from a  $[0,1]$  uniform distribution. As a consequence, to estimate the direction of  $\mathbf{k}$ , in the point of intersection  $P_1$ , the theoretic normal vector  $\mathbf{k}'$  needs to be twofold rotated. The rotation angles are  $\theta_{err}$  and, then,  $\varphi_{err}$ . The former rotation is around a vector orthogonal to the plane where the major ellipse lies, while the latter rotation is around  $\mathbf{k}'$ .

The prediction of the normal vector to the reflective surface, in  $P_1$ , allows to calculate the reflected ray direction,  $\mathbf{r}$ , according to (4) [16].

$$\mathbf{r} = \mathbf{v} - 2 \cdot (\mathbf{k} \times \mathbf{v}) \times \mathbf{k} \quad (4)$$

The point of intersection between  $\mathbf{r}$  and the plane where the target lies allows to find the coordinates of the common point  $P_2$ . If  $P_2$  is inside the target area the ray correctly hits the target, otherwise the ray is lost and the transfer efficiency decreases, i.e. the losses at the target stage. This study does not consider multiple reflection phenomena.

Finally, the distance and mutual position between  $P_2$  and the ellipsoid focus point allows to study the radiative incident flux distribution on the target area.

### III. MONTE CARLO SIMULATION

Several geometric and optic parameters affect the global transfer efficiency of solar simulator systems. A list of them, classified according to the physical component they belong to, is provided in the following.

Light source (generally an high flux arc lamp)

- Shape and dimensions;
- Emission light spectrum;
- Emission surface shape and dimensions, e.g. sphere, cylinder, etc.;
- Emission direction distribution;
- Absorption coefficients of quartz bulb and electrodes (if present);
- Interference angle of electrodes (if present).

Ellipsoidal reflective surface

- Reflector shape, identified by the two ellipsoid semi-axes or by the major semi-axis and the truncation diameter;
- Reflector length;
- Absorption coefficient;
- Standard deviation of the dispersion azimuthal angular error distribution.

Target surface

- Shape, e.g. circular, squared, rectangular;
- Dimensions;
- Relative position toward the ellipsoid.

For a given a set of the previous parameters, the geometric and optical features of the solar simulator are univocally identified and the ray-tracing model, described in previous Section II, is applicable to study the global performances of the system. In particular, the simulation of a large number of the emitted light rays allows to assess the expected distribution of the light on the target and to estimate the system global transfer efficiency. Such a simulation is feasible through the well-known Monte Carlo simulative approach when integrated to the described ray-tracing model.

Finally, varying one or several of the previous parameters, through a multi-scenario analysis, the best configuration of the system can be identified. Such a strategy is adopted in the realistic case study described in the following paragraph.

#### 3.1 CASE STUDY. DESIGN OF A SINGLE SOURCE CONCENTRATING SOLAR SIMULATOR

The following case study provides an empirical application of the proposed approach. The design of a small-scale single source concentrating solar simulator is assessed. The system overall structure is similar to that proposed in previous Fig. 1. In particular, the emitting source is a commercial OSRAM XBO® 3000W/HTC OFR xenon short arc lamp with a luminous flux of 130000lumen and an average luminance of 85000cd/cm<sup>2</sup> [17]. The target area is assumed squared, centered on the ellipsoid focus point and its dimensions are of 50×50mm. Such features are assumed constant, while several configurations of the reflector shape, corresponding to different sets of the aforementioned parameters, are tested and the performances compared.

Further details about the considered high flux arc lamp are in Table 1 and represented in Fig. 4. The quartz bulb absorption coefficient is of 4% and the electrode absorption coefficient is of 98%.

Table 1: Geometric Features of the Emitting Source. Notations Refer to Fig. 4.

Lamp length (overall)	$l_1$	398mm
Lamp length	$l_2$	350mm
Lamp cathode length	$a$	165mm
Electrode gap (cold)	$eo$	6mm
Bulb diameter	$d$	60mm
Electrode interference angles	$\vartheta_1$	30°
	$\vartheta_2$	20°

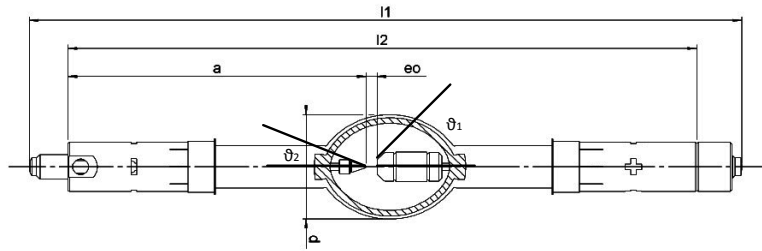


Figure 4: High Flux Arc Lamp Geometry.

Considering the ellipsoidal mirror reflector, the next Table 2 summarizes the tested scenarios corresponding to different geometric shapes and optic performances. The ranges of variation and the incremental steps for four of the most relevant parameters are presented.

Table 2: Tested Configurations for the Ellipsoidal Reflector [mm]. Refer to Fig. 2 for Notations.

	Min value	Max value	Step
$A$	200	1000	100
$TD$	100	$2A$	50
$\sigma_{err}$	0.005	0.01	0.005
$L$	$A - \sqrt{A^2 - TD^2}/4$	$A$	50

Furthermore, a constant mirror absorption coefficient of 4% is considered in the analysis. 3840 scenarios appear and are simulated, i.e. multi-scenario analysis. For each scenario,  $N = 5 \times 10^5$  emitted rays are traced and the results collected.

#### IV. RESULTS AND DISCUSSION

The measurement of the performances for each simulated scenario is assessed collecting the following data:

- $N_A$ , number of the rays absorbed by the light source;
- $N_H$ , number of the rays lost due to the presence of the hole used to install the light source;
- $N_L$ , number of the rays falling out of the reflector shape;
- $N_R$ , number of the rays absorbed by the mirror reflector;
- $N_T$ , number of the reflected rays hitting the target;
- $N_O$ , number of the reflected rays that do not hit the target.

Such a data allow to calculate the following key performance indicators highlighting the impact of the reflector features on the solar simulator efficiency:

- Losses due to the reflector shape, i.e. the ellipsoid shape and eccentricity, the hole and the truncation diameters;

$$\xi_1 = \frac{N_H + N_L}{N - N_A} \tag{5}$$

- Losses due to the optic and distortion effects caused by the reflector surface error distribution;

$$\xi_2 = \frac{N_R + N_O}{N - N_A - N_H - N_L} \tag{6}$$

- Global reflector transfer efficiency;

$$\eta = (1 - \xi_1) \cdot (1 - \xi_2) = \frac{N_T}{N - N_A} \tag{7}$$

- Statistical distribution of the reflected rays on the target surface, i.e. the mean distance  $M_D$  and its standard deviation  $\sigma_D$  between the point of intersection  $P_2$  and the target center.

The Table 3 shows a subset of the obtained results for the tested scenarios presenting the twenty best and worst cases. In addition to the previous notations,  $\varepsilon$  indicates the ellipsoidal reflector eccentricity, as in (8), and included in the [0,1] range.

$$\varepsilon = \sqrt{1 - B^2/A^2} \tag{8}$$

Furthermore, Fig. 5 shows an example of radiative flux map. It considers the best of the simulated scenarios. The squared dashed line identifies the target surface whereas all dots inside the square are the rays hitting the target. The other dots are the rays causing the losses at the target stage.

Table 3: Multi Scenario Analysis Results. Twenty Best and Worst Scenarios.

Rank	A	TD	$\sigma_{err}$	L	B	$\epsilon$	$N_A$	%	$N_H$	%	$N_L$	%	$N_R$	%	$N_T$	%	$N_o$	%	$\xi_1$	$\xi_2$	$\eta$	$M_D$	$\sigma_D$
1	600	650	0.005	600	325	0.841	65506	B.10%	5585	1.2%	6771	1.35%	16942	3.39%	401501	80.30%	3695	0.74%	2.844%	4.889%	92.407%	8.284	6.387
2	700	700	0.005	700	350	0.866	65865	B.17%	6287	1.26%	719	0.14%	16935	3.39%	399723	79.94%	10471	2.09%	1.614%	6.416%	92.073%	9.867	7.265
3	700	750	0.005	700	375	0.844	65477	B.10%	2107	0.42%	5849	1.17%	17211	3.44%	399732	79.95%	9624	1.92%	1.831%	6.291%	91.993%	9.622	7.147
4	600	600	0.005	600	300	0.866	65943	B.19%	13355	2.67%	702	0.14%	16782	3.36%	399052	79.81%	4166	0.83%	3.239%	4.988%	91.935%	8.521	6.205
5	600	700	0.005	600	350	0.812	65936	B.19%	1491	0.30%	13675	2.74%	16838	3.37%	398989	79.80%	3071	0.61%	3.494%	4.753%	91.919%	8.077	7.453
6	500	550	0.005	500	275	0.835	65626	B.13%	12034	2.41%	7907	1.58%	16699	3.34%	396935	79.39%	799	0.16%	4.591%	4.222%	91.381%	6.918	5.108
7	500	600	0.005	500	300	0.800	65623	B.12%	4064	0.81%	16235	3.25%	16688	3.34%	396752	79.35%	638	0.13%	4.673%	4.184%	91.338%	6.705	5.281
8	700	800	0.005	700	400	0.821	65424	B.08%	499	0.10%	11629	2.33%	17004	3.40%	396659	79.33%	8785	1.76%	2.791%	6.105%	91.275%	9.462	7.226
9	600	650	0.005	550	326	0.839	65174	B.03%	5308	1.06%	13451	2.69%	16698	3.34%	395752	79.15%	3617	0.72%	4.314%	4.883%	91.014%	8.298	6.631
10	700	700	0.005	650	351	0.865	65824	B.16%	6088	1.22%	5619	1.12%	16789	3.36%	395000	79.00%	10680	2.14%	2.696%	6.502%	90.977%	9.868	7.868
11	700	750	0.005	650	376	0.844	65819	B.16%	1925	0.39%	11180	2.24%	16775	3.36%	394742	78.95%	9559	1.91%	3.018%	6.254%	90.916%	9.661	12.983
12	600	600	0.005	550	301	0.865	65393	B.08%	13003	2.60%	6290	1.26%	16493	3.30%	394753	78.95%	4068	0.81%	4.439%	4.951%	90.830%	8.508	6.197
13	800	800	0.005	800	400	0.866	65306	B.06%	2336	0.47%	744	0.15%	17232	3.45%	394171	78.83%	20211	4.04%	0.709%	8.675%	90.678%	11.228	8.321
14	600	750	0.005	600	375	0.781	65675	B.14%	286	0.06%	21051	4.21%	16654	3.33%	393652	78.73%	2682	0.54%	4.913%	4.682%	90.635%	7.923	10.472
15	800	850	0.005	800	425	0.847	65715	B.14%	659	0.13%	5146	1.03%	17002	3.40%	392510	78.50%	18968	3.79%	1.337%	8.395%	90.381%	11.004	8.655
16	600	700	0.005	550	351	0.811	65720	B.14%	1407	0.28%	21106	4.22%	16375	3.28%	392244	78.45%	3148	0.63%	5.184%	4.741%	90.321%	8.074	6.300
17	700	850	0.005	700	425	0.795	65720	B.14%	211	0.04%	17598	3.52%	16642	3.33%	392119	78.42%	7710	1.54%	4.101%	5.847%	90.292%	9.232	10.141
18	700	650	0.005	650	326	0.885	65836	B.17%	13360	2.67%	584	0.12%	16704	3.34%	391884	78.38%	11632	2.33%	3.212%	6.743%	90.262%	10.109	7.391
19	700	650	0.005	700	325	0.886	65749	B.15%	13333	2.67%	512	0.10%	16895	3.38%	391933	78.39%	11578	2.32%	3.188%	6.773%	90.255%	10.112	7.375
20	500	500	0.005	500	250	0.866	65597	B.12%	24369	4.87%	722	0.14%	16449	3.29%	391887	78.38%	976	0.20%	5.776%	4.257%	90.213%	7.188	6.463
3821	600	450	0.005	50	563	0.346	65447	B.09%	35	0.007%	409130	81.83%	1016	0.20%	24347	4.87%	25	0.01%	94.158%	4.100%	5.603%	53.826	4427
3822	600	450	0.01	50	563	0.346	65927	B.19%	23	0.005%	408554	81.71%	1053	0.21%	22152	4.43%	2291	0.46%	94.126%	13.16%	5.103%	128.611	23924
3823	1000	850	0.005	100	975	0.222	65157	B.03%	11	0.002%	411962	82.39%	897	0.18%	21344	4.27%	629	0.13%	94.741%	6.672%	4.908%	92.488	5811
3824	800	500	0.005	50	718	0.440	65429	B.09%	22	0.004%	412160	82.43%	911	0.18%	21118	4.22%	360	0.07%	94.848%	5.677%	4.860%	43.496	2531
3825	900	800	0.01	100	873	0.243	65717	B.14%	11	0.002%	406282	81.26%	1085	0.22%	20798	4.16%	6107	1.22%	93.555%	25.695%	4.789%	383.653	150438
3826	1000	1050	0.01	150	997	0.082	66030	B.21%	8	0.002%	406182	81.24%	1177	0.24%	20351	4.07%	6252	1.25%	93.599%	26.742%	4.689%	199.142	7646
3827	900	500	0.01	50	761	0.535	65500	B.10%	23	0.005%	407282	81.46%	1145	0.23%	17951	3.59%	8099	1.62%	93.741%	33.992%	4.131%	58.225	2676
3828	1000	500	0.01	50	801	0.599	65804	B.16%	12	0.002%	403926	80.79%	1218	0.24%	17887	3.58%	11153	2.23%	93.031%	40.885%	4.120%	28.040	65
3829	800	500	0.01	50	718	0.440	65880	B.18%	27	0.005%	411665	82.33%	937	0.19%	16543	3.31%	4948	0.99%	94.834%	26.240%	3.811%	75.963	5461
3830	1000	550	0.005	50	881	0.474	66168	B.23%	12	0.002%	415741	83.15%	730	0.15%	16257	3.25%	1092	0.22%	95.833%	10.078%	3.747%	53.311	5468
3831	1000	850	0.01	100	975	0.222	65330	B.07%	12	0.002%	412098	82.42%	871	0.17%	15910	3.18%	5779	1.16%	94.810%	29.477%	3.660%	256.684	37704
3832	700	500	0.005	50	674	0.272	65630	B.13%	19	0.004%	419413	83.88%	589	0.12%	14309	2.86%	40	0.01%	96.561%	4.211%	3.294%	71.500	12637
3833	900	550	0.005	50	837	0.368	65986	B.20%	18	0.004%	420144	84.03%	543	0.11%	12947	2.59%	362	0.07%	96.808%	6.533%	2.983%	55.009	2629
3834	700	500	0.01	50	674	0.272	65828	B.17%	14	0.003%	418994	83.80%	585	0.12%	12729	2.55%	1850	0.37%	96.507%	16.058%	2.932%	100.957	3266
3835	1000	550	0.01	50	881	0.474	65808	B.16%	16	0.003%	416421	83.28%	687	0.14%	11242	2.25%	5826	1.17%	95.911%	36.683%	2.589%	91.629	6668
3836	900	550	0.01	50	837	0.368	65775	B.16%	16	0.003%	420351	84.07%	558	0.11%	9775	1.96%	3525	0.71%	96.809%	29.463%	2.251%	135.650	13985
3837	1000	600	0.005	50	961	0.277	65848	B.17%	8	0.002%	427627	85.53%	269	0.05%	6052	1.21%	196	0.04%	98.499%	7.135%	1.394%	101.737	18564
3838	800	550	0.005	50	790	0.156	65524	B.10%	11	0.002%	428332	85.67%	236	0.05%	5867	1.17%	30	0.01%	98.588%	4.337%	1.350%	87.917	8513
3839	800	550	0.01	50	790	0.156	65207	B.04%	7	0.011%	428814	85.76%	251	0.05%	4882	0.98%	839	0.17%	98.626%	18.252%	1.123%	195.014	16000
3840	1000	600	0.01	50	961	0.277	65586	B.12%	11	0.002%	427651	85.53%	296	0.06%	4658	0.93%	1798	0.36%	98.446%	31.013%	1.072%	226.342	40309

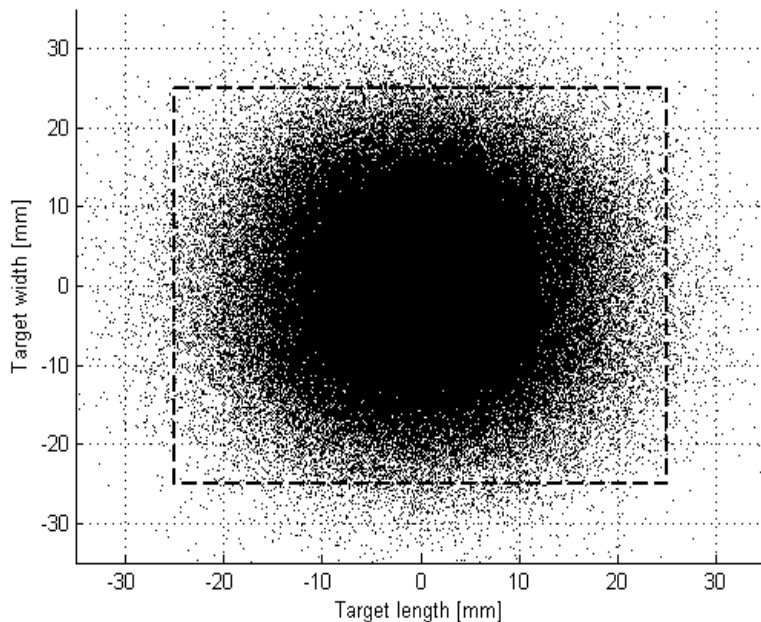


Figure 5: Radiative Flux Map for the Best Scenario.

The values of the global transfer efficiency vary from 92.407% of the best scenario to 1.072% of the worst case. Consequently, a first relevant outcome of the analysis is the heavily influence of the reflector design on the solar simulator performances.

Considering the best scenarios, the  $\xi_1$  and  $\xi_2$  loss indices present values lower than 9%, and the large amount of the reflected rays are concentrated close to the target, i.e. the mean distance between the rays and the ellipsoid focus point,  $M_D$ , is close to 10mm and the standard deviation,  $\sigma_D$ , is included between [5,13]mm. On the contrary, the most relevant cause for the performance decrease is the reflector shape losses. With reference to the worst scenarios, high values of  $\xi_1$ , i.e. greater

than 93%, are always experienced, while  $\xi_2$  does not present a regular trend. Such losses depend on the length of the reflector, i.e. the aforementioned parameter  $L$ . All the worst scenarios present little values for such a parameter, e.g. 50-100mm, so that the majority of the emitted rays is lost because no intersection with the mirror surface occurs. The high number of the rays falling out of the reflector shape,  $N_L$ , included between 80% and 86%, clearly highlights this evidence.

Furthermore, the standard deviation of the dispersion azimuthal angular error distribution,  $\sigma_{err}$ , represents another relevant parameter affecting the global performances of the system. As expected, the lower  $\sigma_{err}$ , the higher the global transfer efficiency values are. The standard deviation error depends on the accuracy of the reflector manufacturing. The decrease of this parameter is generally associated to the increase of the reflector production costs. Fig. 6 correlates the reflector length to the global transfer efficiency for the two simulated values of  $\sigma_{err}$ , i.e. 0.005mm and 0.01mm.

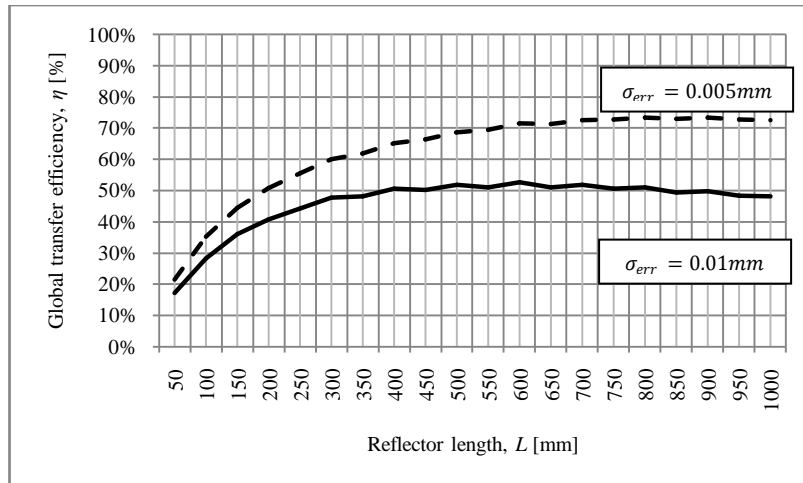


Figure 6: Correlation between the Reflector Length and the Global Transfer Efficiency for the Two Values of  $\sigma_{err}$ .

The results present similarities in the waveforms. Low values of the reflector length are associated to poor performances, i.e.  $\eta < 30\%$ . Optimal conditions are, respectively, for a reflector length of 800mm and  $\sigma_{err} = 0.005\text{mm}$  and of 600mm for  $\sigma_{err} = 0.01\text{mm}$ . A significant performance increase occurs for values of  $L$  included in  $[50,450]\text{mm}$  range, while for the higher values of the reflector length, i.e.  $L > 500\text{mm}$ , the global transfer efficiency presents comparable values. Finally, considering the gap between the performances in the trends identified by the two values of  $\sigma_{err}$ , an increase, from 4.241% to 24.466%, occurs. High values of  $\sigma_{err}$  have a crucial impact on the global transfer efficiency in presence of high values of  $L$ . In fact, long reflectors force the emitted rays to sweep out long trajectories from the source to the mirror and, then, from the mirror to the target. An anomaly in the trajectories generates an angular deviation of the ray path. Such a deviation is amplified by the distance between the mirror and the target. Consequently, if  $L$  increases the standard deviation of the dispersion azimuthal angular error distribution must have low values not to significantly reduce  $\eta$ .

Another relevant parameter affecting the mirror reflector design is the ellipsoid eccentricity,  $\epsilon$ , defined in previous (8) and included in the  $[0,1]$  range. It identifies the mutual position of the vertices and the foci. If  $\epsilon$  is equal to 0 the ellipsoid is a sphere, i.e.  $A = B$ . Values of  $\epsilon$  between 0 and 1 are for eccentric geometries in which  $B < A$ . If  $\epsilon = 1$  the ellipsoid degenerates into a plane and the foci lay upon the vertices on the major axis. The developed multi-scenario analysis highlights a range of the optimal values for the ellipsoid eccentricity included between 0.75 and 0.9, as in Fig. 7, correlating the ellipsoidal mirror eccentricity to the values of  $\eta$ . Each dot represents one of the 3840 simulated scenarios.

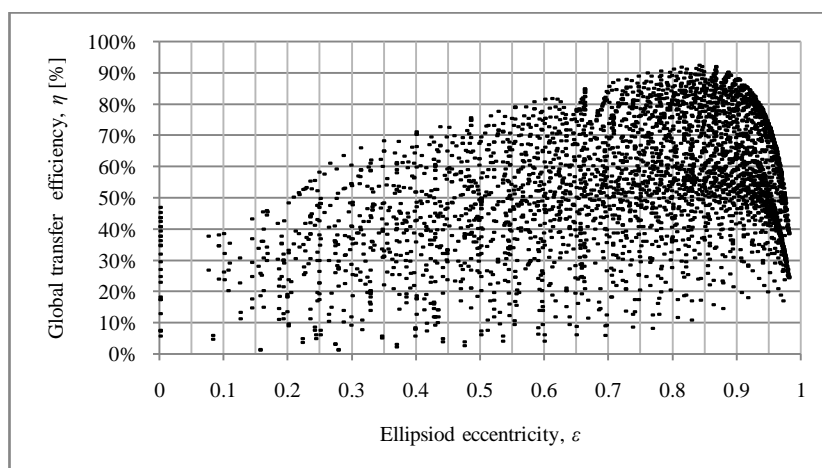


Figure 7: Correlation between the Ellipsoid Eccentricity and Global Transfer Efficiency.

This outcome may be in contrast to the major literature evidences suggesting low values of  $\varepsilon$  to maximize the reflector global transfer efficiency [16,18]. On the contrary, in the proposed analysis values of eccentricity close to zero generate the worst performances. A reasonable explanation for this evidence lies in the adopted reflector modeling approach. The literature ray-tracing models and related results approximate the reflector with an ellipsoid of revolution neglecting both the truncation section, i.e. the previously called  $TD$  parameter, and the hole necessary to install the light source. The proposed ray-tracing approach includes these two elements in the analytical model to provide a realistic and accurate description of the physical system. The presence of these elements significantly modifies the geometric and optic features of the solar simulator introducing the so-called losses at the reflector stage (see Fig. 3) that significantly contribute to the global transfer efficiency decrease, especially for the scenarios in which  $L$  and  $\varepsilon$  assume low values (see Table 3). In fact, if  $\varepsilon$  is low the foci are located far from the vertices and close to the ellipsoid geometric center, i.e. the point of intersection of the two axes. In this circumstance, the light source juts out from the reflector profile and a large number of the emitted rays does not hit the reflector surface. The lower the reflector length, the higher such losses are.

On the contrary, in eccentric reflectors the light source is close to the ellipsoid major axis vertex and a lower number of rays is lost. However, very high values of  $\varepsilon$ , i.e.  $\varepsilon > 0.9$ , cause a further increase of the losses at the reflector stage and a decrease of  $\eta$ . This is due to the presence of the hole for the light source installation. A focus point located close to the reflector vertex increases the value of  $N_H$ , i.e. the number of the rays lost due to the presence of the hole used to install the light source, so that, also in this case, the global transfer efficiency decreases. As introduced before, optimal values for the reflector eccentricity are in the [0.75,0.9] range.

## V. CONCLUSIONS AND FURTHER RESEARCH

This paper presents an approach facing the effective design of solar simulators. The developed model reproduces the trajectories of the light rays considering the main physical and optic phenomena that occur from the source to the target area. The ellipsoidal reflector geometries are focused. In particular, the solar simulator reflector is a truncated ellipsoid of revolution with the light source located on one focus point and the target area on the other. The proposed ray-tracing model is integrated to a Monte Carlo simulation to study and compare the performances of several reflector geometries. A case study, based on a commercial xenon short arc lamp, is described simulating 3840 scenarios and varying four major parameters affecting the quality and reflectivity of the mirror surface, i.e. the ellipsoid major axis, the truncation diameter, the reflector length and the standard deviation of the azimuthal angular error distribution. For each simulated scenario, the data about the losses and the number of rays on target are collected and summarized in the three key performance indices proposed in (6) to (9) together with a statistic analysis of the distribution of rays on the target.

The main outcomes highlight the relevance of the proper design of the reflector shape to obtain high values of the global transfer efficiency. The gap between the best and worst scenarios is higher than 90%. Furthermore, correlations between the four considered parameters are highlighted. As example, high values of the reflector length, in presence of high values of the standard deviation of the azimuthal angular error distribution, amplify the global transfer efficiency decrease, while, low values of the ellipsoid eccentricity cause an increase of the lost rays.

The obtained parameter values, for the best scenario, are of 600mm for both the ellipsoid major semi-axis and reflector length, 325mm for the minor semi-axis and  $\sigma_{err}$  equals to 0.005mm. For this scenario, the global transfer efficiency is 92.407% while the distribution of rays on the target area presents a mean distance from the ellipsoid focus point of 8.284mm and a standard deviation of 6.387mm.

Both the model description and its application to the realistic case study convey to point out the interest of the proposed approach for scientists and practitioners. Its application before the system development and manufacture allows to simulate the system behavior and to assess the expected performances. Furthermore, the inclusion of the operative geometric constraints, e.g. the truncation diameter, the lamp installation hole, etc., to the ray-tracing model increases the approach applicability overcoming the assumptions of several of the models proposed by the recent literature.

Further research deals with a validation of the case study results through the development of the solar simulator and a further field-campaign. To this purpose, the authors already purchased the ellipsoidal reflector and they are now developing the overall structure of the solar simulator to collect the experimental data to be compared to the evidences coming from the proposed approach. At last the enlargement of the approach to multi source solar simulators and the inclusion of multiple reflection phenomena is encouraged.

## REFERENCES

- [1] J. Petrash, P. Coray, M. Meier, M. Brack, P. Häberling, D. Wuillemin, and A. Steinfeld, A novel 50 kW 11,000 suns high-flux solar simulator based on an array of xenon arc lamps, *Journal of Solar Energy Engineering*, 129, 2007, 405-411M.
- [2] C. Domínguez, I. Antón, and G. Sala, Solar simulator for concentrator photovoltaic systems, *Optics express*, 16(19), 2008, 14894–14901.
- [3] C. Domínguez, S. Askins, I. Antón, and G. Sala, Characterization of five CPV module technologies with the Helios 3198 solar simulator, *IEEE*, 2009, 1004–1008.
- [4] M. Pravettoni, R. Galleano, E.D. Dunlop, and R.P. Kenny, Characterization of a pulsed solar simulator for concentrator photovoltaic cell calibration, *Measurement Science and Technology*, 21, 2010, 1-8.
- [5] H. Renh, and U. Hartwig, A solar simulator design for concentrating photovoltaics, *Proc. SPIE The International Society for Optical Engineering*, San Diego, CA, 2010, 1-4.
- [6] F. Hussain, M.Y.H. Othman, B. Yatim, H. Ruslan, and K. Sopian, Fabrication and irradiance mapping of low cost solar simulator for indoor testing of solar collector, *Journal of Solar Energy Engineering*, 133(4), 2011, 44502 1–4.

- [7] Q. Meng, Y. Wang, and L. Zhang, Irradiance characteristics and optimization design of a large-scale solar simulator, *Solar Energy*, 85, 2011, 1758-1767.
- [8] H. Amoh, Design for multi-solar simulator, Proc. SPIE The International Society for Optical Engineering, Denver, CO, 2004, 192-199.
- [9] Q. Meng, and Y. Wang, Testing and design of a low-cost large scale solar simulator, Proc. SPIE The International Society for Optical Engineering, San Diego CA, 2011, 8128.
- [10] K.R. Kruger, J.H. Davidson, and W. Lipiński, Design of a new 45 kWe high-flux solar simulator for high-temperature solar thermal and thermo-chemical research, *Journal of Solar Energy Engineering*, 133(4), 2011, 11013 1-8.
- [11] D.S. Codd, A. Carlson, J. Rees, and A.H. Slocum, A low cost high flux solar simulator, *Solar Energy*, 84, 2010, 2202-2212.
- [12] G. Johnston, On the analysis of surface error distributions on concentrated solar collectors, *Transactions of the ASME*, 117, 1995, 294-296.
- [13] C.F. Chen, C.H. Lin, and H.T. Jan, A solar concentrator with two reflection mirrors designed by using a ray tracing method, *Optik*, 121, 2010, 1042-1051.
- [14] Y. Ota, and K. Nishioka, 3-dimensional simulator for concentrator photovoltaic modules using ray-trace and circuit simulator, Proc. 35th IEEE Photovoltaic Specialists Conference, PVSC 2010, Honolulu, HI, 3065-3068.
- [15] T. Cooper, and A. Steinfeld, Derivation of the angular dispersion error distribution of mirror surfaces for Monte Carlo ray-tracing applications, *Journal of Solar Energy Engineering*, 133(4), 2011, 44501 1-4.
- [16] A. Steinfeld, Exchange factor between two spheres placed at the foci of a specularly reflecting ellipsoidal cavity, *International Communications in Heat and Mass Transfer*, 18, 1991, 19-26.
- [17] Osram, Technical information No. 5264, Available on-line: <http://www.osram.com> [accessed January 2013].
- [18] A. Steinfeld, and E.A. Fletcher, Solar energy absorption efficiency of an ellipsoidal receiver-reactor with specularly reflecting walls, *Energy*, 13(8), 1988, 609-614.